

THE X-RAY SURFACE BRIGHTNESS DISTRIBUTION FROM DIFFUSE GAS

GREG L. BRYAN¹

Department of Physics, Massachusetts Institute of Technology, Cambridge, MA 02139

AND

G. MARK VOIT

Space Telescope Science Institute, 3700 San Martin Drive, Baltimore, MD 21218

Draft version October 27, 2018

ABSTRACT

We use simulations to predict the X-ray surface brightness distribution arising from hot, cosmologically distributed diffuse gas. The distribution is computed for two bands: 0.5-2 keV and 0.1-0.4 keV, using a cosmological-constant dominated cosmology that fits many other observations. We examine a number of numerical issues such as resolution, simulation volume and pixel size and show that the predicted mean background is sensitive to resolution such that higher resolution systematically increases the mean predicted background. Although this means that we can compute only lower bounds to the predicted level, these bounds are already quite restrictive. Since the observed extra-galactic X-ray background is mostly accounted for by compact sources, the amount of the observed background attributable to diffuse gas is tightly constrained. We show that without physical processes in addition to those included in the simulations (such as radiative cooling or non-gravitational heating), both bands exceed observational limits. In order to examine the effect of non-gravitational heating we explore a simple modeling of energy injection and show that substantial amounts of heating are required (i.e. 5 keV per particle when averaged over all baryons). Finally, we also compute the distribution of surface brightness on the sky and show that it has a well-resolved characteristic shape. This shape is substantially modified by non-gravitational heating and can be used as a probe of such energy injection.

Subject headings: cosmology: theory, intergalactic medium

1. INTRODUCTION

The X-ray background has now been largely resolved into individual point sources (e.g. Hasinger et al. 1993; Mushotzky et al. 2000), the majority of which are thought to be AGN (e.g. Boyle 1994). This constrains the amount of the background which may be due to a diffuse hot intergalactic medium (Barcons, Fabian & Rees 1991). Recent work has applied these ideas specifically to the soft X-ray background, arguing that currently popular cosmological models predict too much flux and so require some non-gravitational heating to reduce the emissivity (Pen 1999; Wu, Fabian & Nulsen 2000b). However, since the emission process (primarily Bremsstrahlung) is sensitive to temperature and particularly density, it is necessary to have a good prediction of the density and temperature distribution of the diffuse gas. To date, most work on this subject has adopted semi-analytic techniques or made strong assumptions about the temperature distribution of the gas. It has lately become possible (although as we will show still difficult) to use numerical simulations to model the distribution of gas in the universe and so directly predict its X-ray emissivity.

Beyond a simple number — the mean background — it is of interest to predict other facets of the diffuse X-ray background, such as its distribution function. This last quantity tells us how much of the sky has a given surface brightness and can be used to investigate the superposition of multiple sources along the line of sight during

cluster or group observations, or during searches for filaments (Voit, Evrard & Bryan 2000). It is also a probe of the physics of galaxy formation, as its shape is sensitive to non-gravitational heating from, for example, supernovae and AGN. A number of groups have examined the spatial correlation of the X-ray background with other objects (e.g. Soltan et al. 1999), and although we do not do so here, it would also be of interest to investigate the predicted clustering properties of the diffuse X-ray background (e.g. Croft et al. 2000).

In this paper, we draw on the results of hydrodynamic simulations to compute the distribution of surface brightness in two bands on the X-ray sky, neglecting the contribution from point sources. Since the simulation boxes are relatively small compared to the line-of-sight distance, we generate the distribution by effectively stacking the simulations. The method for doing this is described in section 2. Using this algorithm, we show, in section 3, the results from a number of simulations, examining the effect of resolution and comparing to previous work on this subject. Finally, we investigate the effect of additional physical processes, such as cooling and non-gravitational heating (from, for example, supernovae).

In a previous paper (Voit, Evrard & Bryan 2000), we have discussed how the diffuse X-ray background can be a source of confusion for group observations as well as during searches for filamentary gas. In a related paper (Voit & Bryan 2000), we discuss these distributions in the context of a simple analytic model which accurately reproduces

¹Hubble Fellow

the simulation results, as well as examining the role point sources play in the distribution.

2. COMPUTING THE X-RAY BACKGROUND

In order to compute the X-ray background from the diffuse gas, we must know the distribution of density and temperature along the line-of-sight. Rather than compute this in a single step, we break down the computation into two steps. In the first, we simulate a cubic region of the universe, using a numerical hydrodynamics code (described below). The results of these simulations are saved at various points during the computation, and each output can be used to generate a map of X-ray emission from that particular region, at that redshift. In the second step, we develop an algorithm to statistically combine these maps (or rather, the surface brightness distributions computed from them) to generate the final distribution.

2.1. The Simulations

The density and temperature distribution is computed by solving the equations of hydrodynamics in a comoving volume of side length L . An adaptive mesh refinement (AMR) technique is used to solve these equations. This algorithm is described elsewhere (Bryan 1999; Bryan & Norman 1997, 1999; Norman & Bryan 1998), but we briefly summarize it here. The dark matter is simulated by following particle trajectories, while the baryon fluid is modeled by discretizing the density, temperature and velocity distributions onto a mesh. The discretized equations of hydrodynamics are solved using a piece-wise parabolic method, modified for cosmology (Colella & Woodward 1984; Bryan et al. 1995). The gravitational acceleration comes from solving Poisson's equation on the mesh, using an iterated multi-grid technique.

As objects collapse and form, the code must resolve smaller and smaller length scales. This is accomplished in AMR by overlaying additional, finer meshes onto areas that require improved resolution as the simulation proceeds. These finer meshes have a cell spacing $1/2$ as large as the coarser grids from which they obtain their boundary conditions. This procedure can be repeated recursively, with finer and finer meshes covering less and less volume. The cell spacing on any given level l (where $l = 0$ refers to the top grid) is given by $\Delta x = L/(2^l N)$, where N is the number of mesh points per dimension on the top grid. The refinement criterion is designed to keep a fixed mass resolution: additional grids are added whenever the mass (either baryonic or dark) in a cell exceeds a certain threshold, chosen to be four times the initial mass in a cell.

The simulation is initialized at high redshift ($z = 30$), when the perturbations are nearly linear. In this work, we restrict ourselves to a single cosmological model, one which matches a large number of current observations. The ratio of the density in non-relativistic matter to the critical density is taken to be $\Omega_0 = 0.3$. The model is flat, with a cosmological constant energy density $\Omega_\Lambda = 0.7$ and Hubble constant $h = 0.67$, where h is in units of 100 km/s/Mpc . The baryon fraction was taken to be $\Omega_b = 0.04$, which is slightly on the low side of current estimates (Burles & Tytler 1999). The power spectrum of initial density perturbations is taken from Eisenstein & Hu (1998), which we normalize so that the *rms* fluctuations in spheres of $8 h^{-1} \text{ Mpc}$ is $\sigma_8 = 0.9$.

In this paper, we will analyze the results from a number of simulations with varying resolutions and box sizes in order to investigate numerical uncertainties. The parameters for these runs are shown in Table 1, along with designated name for each simulation. In each case, we list the box size (L), the number of grid point per dimension on the top grid (N_{grid}), the highest resolution reached in the mesh refinement (in each case we go down four levels). Finally, the last two simulations include a very simple heating scenario designed to investigate the effect of feedback. In this run, we increased the gas temperature by 1 keV at $z = 3$ (an increase of 1.5 keV per particle). Although this is obviously overly simplified, it is a straightforward way to show the effect of increasing the gas entropy on the X-ray background.

2.2. Computing the distribution

We compute the surface brightness distribution in the following way. First, for each simulation output at a redshift z , we compute a surface brightness map by integrating along lines-of-sight from one edge of the volume to the other:

$$S(z, \Delta z) = \frac{1}{4\pi(1+z)^4} \int \epsilon(T) n_e n_H dl, \quad (1)$$

where $\epsilon(T)$ is the emissivity in the (appropriately redshifted) X-ray band of interest, n_e is the electron density and n_H is the proton density. The electron and proton densities are computed assuming complete ionization, which is an excellent approximation for the hot gas producing the emission. The emissivity is computed with a Raymond-Smith (1977; 1992 version) code assuming a constant metallicity of 0.3 solar (as we will show below, most of the background comes from groups and clusters at moderate redshifts so this is a very reasonable approximation). An example of such a map is shown in Figure 1.

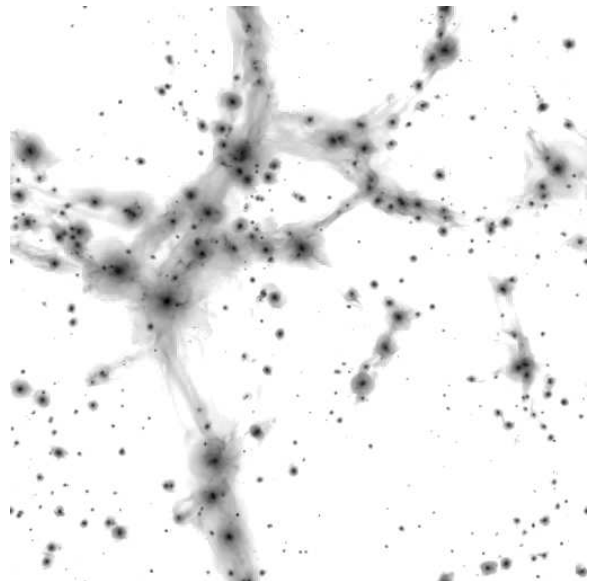


FIG. 1.— A simulated $0.5\text{-}2 \text{ keV}$ X-ray surface brightness map from a region $50 h^{-1} \text{ Mpc}$ on a side at redshift $z = 0.4$ and line-of-sight distance $\Delta z = 0.02$. The greyscale is logarithmic in order to bring out the low surface brightness filaments and ranges from 10^{-21} to $10^{-15} \text{ erg cm}^{-2} \text{ s}^{-1} \text{ arcmin}^{-2}$. The image is 178 arcmins on a side. Note that this is the background from diffuse sources only.

TABLE 1
SIMULATIONS ANALYZED IN THIS PAPER

designation	$L(h^{-1}Mpc)$	N_{grid}	$M_{dm}(M_{\odot})$	finest $\Delta x(h^{-1}kpc)$	feedback	$\bar{S}_{0.5-2.0}$	$\bar{S}_{0.1-0.4}$
L100	100	128	7.9×10^{10}	49	no	1.5×10^{-15}	1.2×10^{-15}
L50-	50	64	7.9×10^{10}	49	no	1.4×10^{-15}	1.2×10^{-15}
L50+	50	128	9.9×10^9	24	no	2.5×10^{-15}	2.9×10^{-15}
L20-	20	64	5.1×10^9	19.2	no	3.3×10^{-15}	3.8×10^{-15}
L20+	20	128	6.3×10^8	9.6	no	5.0×10^{-15}	6.8×10^{-15}
L50f-	50	64	7.9×10^{10}	49	yes	4.3×10^{-16}	3.7×10^{-16}
L50f+	50	128	9.9×10^9	24	yes	6.8×10^{-16}	7.5×10^{-16}

NOTE.— L is the simulation box size, N_{grid} is the number of points per dimension in the initial grid, M_{dm} is the dark matter particle mass, Δx is the smallest cell size and \bar{S} is the mean predicted surface brightness in units of $\text{erg cm}^{-2} \text{s}^{-1} \text{arcmin}^{-2}$.

This map is obviously not a complete X-ray image since it only corresponds to the redshift range from $z - \Delta z/2$ to $z + \Delta z/2$, where $\Delta z = L/3000E(z)$ and L is the length of the computational volume in comoving $h^{-1}Mpc$ (this is accurate as long as $\Delta z/z \ll 1$). The cosmological term is $E^2(z) = \Omega(1+z)^3 + \Omega_R(1+z)^2 + \Omega_{\Lambda}$ (the curvature component is defined as $\Omega_R = 1 - \Omega - \Omega_{\Lambda}$; Peebles 1993). Each pixel subtends an angle on the sky of $\theta = \Delta x/D_A$ where Δx is the proper distance between pixels and D_A is the angular diameter distance. We can also smooth the image at this point, to correspond to an instrument with a given resolution. We discuss this point in more detail below; however, for our standard computation, we do not smooth the maps.

From maps such as the one shown in Figure 1, we can compute both the mean surface brightness, $\bar{S}(z, \Delta z)$, but also the full distribution function $dP/dS(S, z, \Delta z)$. Here, $P(S)$ is the probability that a given line-of-sight will have a surface brightness less than S (excluding compact sources). This distribution is normalized such that:

$$\int \frac{dP(S, z, \Delta z)}{dS} dS = 1. \quad (2)$$

In practice, this is computed for 100 logarithmically distributed points from 10^{-21} to $10^{-13} \text{ erg cm}^{-2} \text{ s}^{-1} \text{ arcmin}^{-2}$ so that the distribution we actually generate is $dP/d \ln S(S, z, \Delta z)$. The number of redshifts (z_i) for which we compute distributions varies somewhat, depending on the details of the simulation, but is typically about 20. In Figure 2, we show the individual $dP/dS(S, z, \Delta z)$ for a range of redshifts.

It is relatively easy to compute the mean predicted background, including contributions from all redshifts; this is given by:

$$\bar{S} = \int \frac{d\bar{S}(z)}{dz} dz \quad (3)$$

where the mean surface brightness per unit redshift at a given arbitrary redshift z is linearly interpolated from the tabulated redshifts z_i (i.e. $d\bar{S}_i(z)/dz = \bar{S}_i(z, \Delta z)/\Delta z$). The results are given in Table 1.

The differential distribution is more difficult to compute, however it can be built out of the individual distribution

functions. First, we examine the problem of combining two distributions at different redshifts, z_1 and z_2 . If we make the simplification that the spatial correlations on scales larger than the box size are negligible, then the joint distribution is given by:

$$\frac{dP_J(S)}{dS} = \int_0^S \frac{dP(S', z_1, \Delta z_1)}{dS} \frac{dP(S - S', z_2, \Delta z_2)}{dS} dS'. \quad (4)$$

When performing this numerical integration, some care must be taken due to the logarithmic spacing of the functions. We divide the sum into two parts, split at $S/2$. In the first half ($S' < S/2$), we evaluate the function at the points at which $dP(S', z_1, \Delta z_1)/dS$ was determined. In the second half ($S' > S/2$), the points of the function $dP(S - S', z_2, \Delta z_2)/dS$ are used. This insures that the finest spacing available is used at all times.

This combines two distributions, but it is a natural extension to combine any number, since we can simply re-apply Eq. (4) with the first term replaced by the joint distribution $dP_J(S)/dS$ and the second by a distribution from another redshift z_3 . The result will be referred to as the cumulative distribution $dP_C(S)/dS$.

To systematically stack the simulations, we adopt the following procedure. Starting at redshift $z = 10 - \Delta z_0/2$ (the contribution from larger redshifts is very small, see Figure 3), we set the cumulative distribution to be equal to $dP(S, z_0, \Delta z_0)/dS$. Ideally, we would like to simply be able to stack the simulation boxes so that one end matches the next; however, in general this requires many outputs and, for a statistical determination of the distribution function, it is not necessary. Instead, we take a step in redshift of size $\Delta z(z)$, where $\Delta z(z)$ is linearly interpolated from the outputs at z_i and z_{i+1} which bracket z (i.e. $z_i < z < z_{i+1}$). We convolve the current distribution $dP_C(S)/dS$ with a distribution which is similarly interpolated from the distributions computed at z_i and z_{i+1} . The current redshift, z , is then decreased by the amount $\Delta z(z)$ and the procedure continues. We stop at $z \approx 0.1$, at which point the pixels become very large (and individual sources would be clearly apparent in the X-ray sky). This introduces a small uncertainty in the final background.

In Figure 2, we show the resulting distribution from

the L100 simulation, for the 0.5 to 2.0 keV band. We plot it in two different ways. The first (top panel) shows $dP/d\ln S$, the probability that a given pixel will fall in a given logarithmic interval in surface brightness. Thus we see that most pixels would have a surface brightness of a few $\times 10^{-16}$ erg cm $^{-2}$ s $^{-1}$ arcmin $^{-2}$ (from diffuse emission alone). The second plot shows this quantity weighted by another factor of S in order to show the quantity that is important for computing the mean flux. We see that most of the contribution to the mean comes from pixels with a surface brightness of $\sim 10^{-14}$ erg cm $^{-2}$ s $^{-1}$ arcmin $^{-2}$.

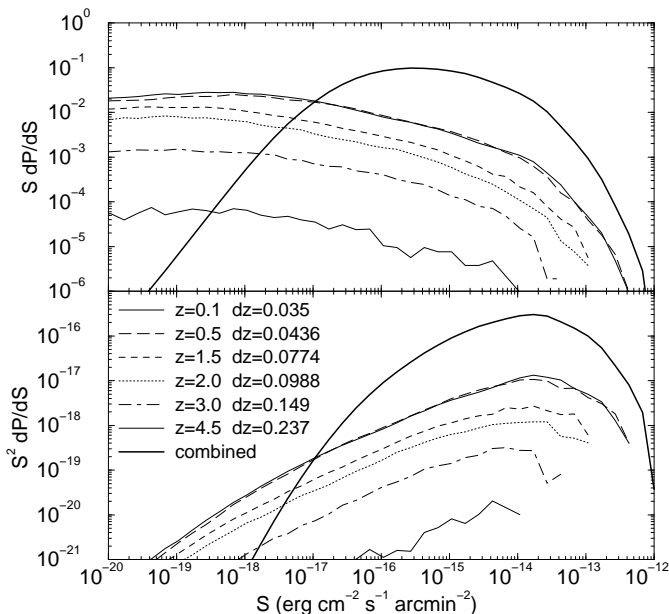


FIG. 2.— The X-ray surface-brightness distribution in the 0.5-2.0 keV band from the L100 simulation. The dashed lines show the contributions from various simulation boxes at the redshifts indicated, while the bold line is the final, composite distribution. The top panel plots SdP/dS in order to show the relative number of pixels per logarithmic interval in surface brightness. The bottom distribution multiplies this by another factor of S to show where the contribution to the mean surface brightness originates.

Comparing the individual distributions (from short redshift ranges) to the cumulative distribution, we can see the effect of stacking. For low surface brightness pixels, the distribution is strongly decreased. This arises simply from the fact that while for a short line of sight (of order $\Delta z \sim 0.03$), it is possible to miss all of the dense knots and filamentary structures seen in Figure 1, it is extremely unlikely for a full line-of-sight. On the high end of the distribution, the shape is preserved while the amplitude increases. This is due to rare, bright pixels for which a single passage through a massive cluster or group dominates the surface brightness contribution. Since multiple passages are rare, increasing the length of the line-of-sight just increases the number of such pixels; their chance of overlap is negligible.

We can double-check the calculation of the distribution by using it to compute the mean, since:

$$\bar{S} = \int S \frac{dP}{dS} dS / \int \frac{dP}{dS} dS \quad (5)$$

Since the distribution and the mean are computed independently (as described above), these two estimates for \bar{S}

should agree. For the larger box (50 and $100h^{-1}$ Mpc), the agreement is very good, within 10%. For the smallest box, the difference is larger, around 20%, as might be expected from the very large number of redshift steps that have to be taken for the smallest simulated box.

In Figure 3, we show how the contribution to the mean flux depends on redshift. Notice that the differential contribution ($d\bar{S}/dz$) is a monotonic function of redshift, implying that most of the contribution comes from relatively low redshifts.

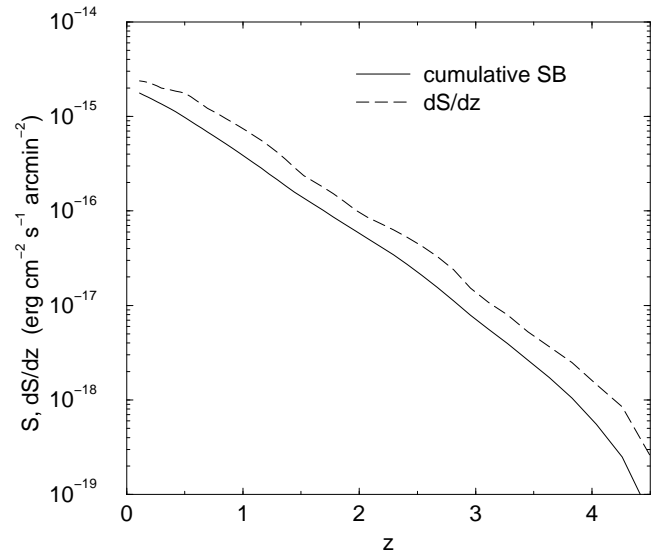


FIG. 3.— This plot shows the mean background diffuse flux as a function of redshift in the 0.5 to 2.0 keV band. The solid line is the cumulative flux (i.e. $\bar{S}(z > z_0)$), while the dashed is the differential contribution ($d\bar{S}/dz$).

3. RESULTS

The mean fluxes for the no-cooling, no-feedback simulations are larger than observed. However, before we draw conclusions from this, we first examine some numerical issues in order to get some idea of the robustness of the result.

3.1. Numerical Issues

The X-ray emitting diffuse gas tends to be distributed on large scales, but because of its density-squared emissivity law, depends sensitively on the small scale distribution within groups, clusters and filaments. This implies that both box size and resolution will be issues. Here we describe a resolution study designed to examine these effects. The different simulation box sizes and resolutions are shown in Table 1, along with the resulting mean background computed using the methods described earlier.

Remarkably, it appears that the results are more sensitive to the resolution of a given simulation, and nearly insensitive to the size of the box (at least for the range considered here). For example, the L100 and L50- simulations differ substantially in the amount of large scale structure which is captured in the simulation, but have the same spatial and mass resolution. Their computed mean background fluxes are nearly identical.

The mass resolution of the simulation appears to be the most important factor. For the background fluxes in the

0.5-2.0 keV band from Table 1 (excluding those with pre-heating), the results can be described by the fitting function:

$$\bar{S} = 2.3 \times 10^{-15} (M_{dm}/10^{10} M_{\odot})^{-0.24} \text{erg cm}^{-2} \text{s}^{-1} \text{arcmin}^{-2}. \quad (6)$$

The correlation coefficient for this fit is very high, 0.996, leaving very little room for other effects such as box size (we note that for even harder bands than considered here, such as 2-10 keV, a larger volume may be important). A naive extrapolation of this trend to infinite resolution predicts an infinite contribution to the soft X-ray background. In reality, the contribution levels off as all the structures that are hot enough to emit in this band are resolved. In fact, it seems plausible that we are very close to this regime, since the virial temperature of a $10^{13} M_{\odot}$ object is about 0.1 keV, which is about the lowest temperature which can contribute significantly to the harder band. At the highest resolution, such objects are resolved with $\sim 10^4$ particles, which experience indicates is the minimum necessary to resolve the central regions where most of the emission originates. See also Bryan & Norman (1998) for a discussion of how numerical resolution affects the predicted X-ray luminosity of clusters. Given this discussion, we can quote only a lower limit to the predicted soft X-ray background from diffuse gas (without pre-heating or radiative cooling):

$$\bar{S}_{0.5-2.0} \geq 5.0 (\Omega_b h^2 / 0.018)^2 \times 10^{-15} \text{erg cm}^{-2} \text{s}^{-1} \text{arcmin}^{-2} \quad (7)$$

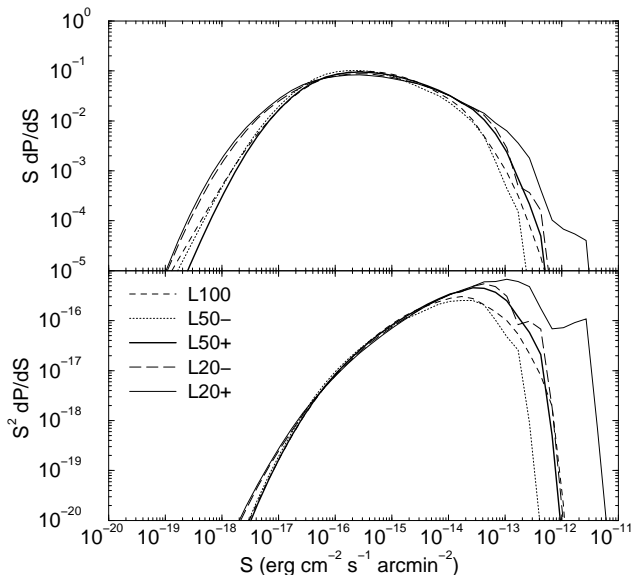


FIG. 4.— The distribution function in the 0.5-2.0 keV band for a variety of simulations with different resolutions. The top and bottom panels have the same meaning as in Figure 2.

In Figure 4, we show the computed distribution functions for some of the simulations described in Table 1 in the 0.5-2.0 keV band. The most striking feature of this plot is the gross similarity among the curves; this is quite reassuring given the very different resolutions and box sizes used. Closer examination reveals a number of systematic trends. First, the range from 10^{-17} to 10^{-14} $\text{erg cm}^{-2} \text{s}^{-1} \text{arcmin}^{-2}$ is quite robust. Below this, in the low surface brightness domain, the two larger box sizes produce

nearly identical results irrespective of resolution, while the $L = 20 h^{-1}$ Mpc simulations show an elevated distribution function (for both resolutions). This demonstrates that the minimum box size to obtain an un-biased sample of the distribution is between 20 and $50 h^{-1}$ Mpc.

For the high surface brightness end, it's clear that resolution plays an important role, with high-resolution simulations producing a larger number of high-brightness pixels. In fact, as we will see, these pixels are primarily produced in the centers of groups and clusters. The bottom panel of Figure 4 shows that it is this high end which determines the mean flux, causing the resolution dependence discussed earlier. The kink at large S values in the L20-curve results from a single cluster, indicating the difficulty in obtaining a fair sample in such a small volume (although note that this single cluster does not make a dominant contribution to the mean surface brightness). Based on this discussion, we have a robust determination of the diffuse background flux distribution below about 10^{-13} $\text{erg cm}^{-2} \text{s}^{-1} \text{arcmin}^{-2}$. Remarkably, this accounts for some 99% of the sky, although the remaining $\sim 1\%$ of the pixels are responsible for setting the mean background. We remind the reader at this point that these simulations include only a minimal physics model, and exclude the effects of both radiative cooling and stellar feedback.

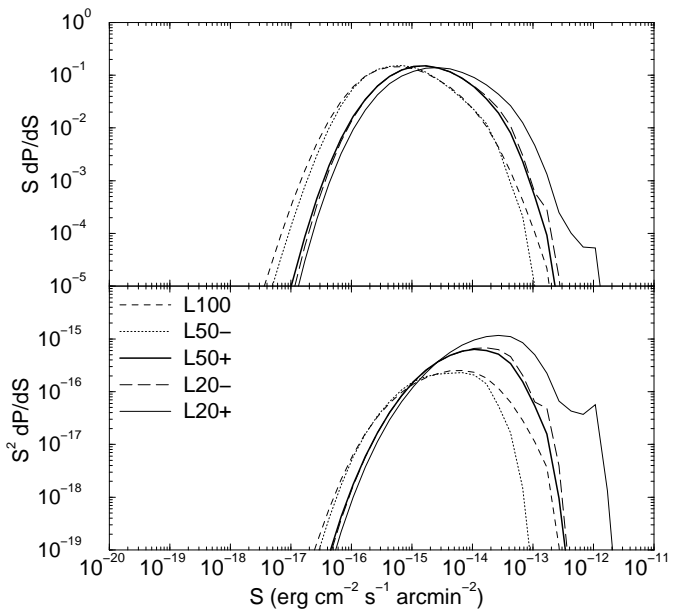


FIG. 5.— The distribution in the 0.1-0.4 keV band function for a variety of simulations with different resolutions.

We now turn to the softer, 0.1-0.4 keV, band. The mean backgrounds given in the last column of Table 1 show the same systematic behaviour with resolution as for the harder band, so again we can estimate only a minimum contribution to the background from diffuse gas (assuming no cooling or re-heating):

$$\bar{S}_{0.1-0.4} \geq 6.8 (\Omega_b h^2 / 0.018)^2 \times 10^{-15} \text{erg cm}^{-2} \text{s}^{-1} \text{arcmin}^{-2} \quad (8)$$

The distribution functions shown in Figure 5 are much more affected by resolution than for the harder band. In fact, as the resolution increases, the entire curve shifts to higher surface brightness levels. The effect of box size is

very small or negligible, even for $L=20 h^{-1}$ Mpc. The resolution effect occurs because the covering factor for the smaller, more numerous objects which contribute to the soft band is nearly unity. Since resolution affects all of these objects (which are small to begin with), the net result is a uniformly brighter background. The unfortunate result is that we cannot robustly predict the background distribution in this band (although it does appear that the shape itself is fairly robust).

3.2. Smoothing the distribution

So far we have focussed on the effect of the simulation resolution on the distribution function of the diffuse X-ray background. However, there are also observational uncertainties which can systematically bias the result. One of these is the removal of point sources, which we will not treat in this paper. However, another which we can address is the effect of artificial smoothing on the sky. This can occur either unintentionally, due to inherent limitations in the resolution of the instrument (X-rays are certainly more difficult to focus than optical photons). However, even for such high-resolution instruments as Chandra, there may be reasons to introduce smoothing as a post processing step. This might be done to improve the photon statistics in areas of the sky with very low surface-brightness.

Figure 6 shows the effect of various amounts of smoothing on the 0.5-2.0 keV distribution of the L50+ simulation. In each case, we have smoothed the distribution with a Gaussian kernel with widths ranging from 0 up to 180 arcsecs. Predictably, the upper and lower ends of the distribution are truncated and with 180" smoothing the sky shows only gentle fluctuations. This confirms the visual impression in the maps shown earlier that the smallest features (generally the peaks of some clusters and groups) are only a few arcsecs in size.

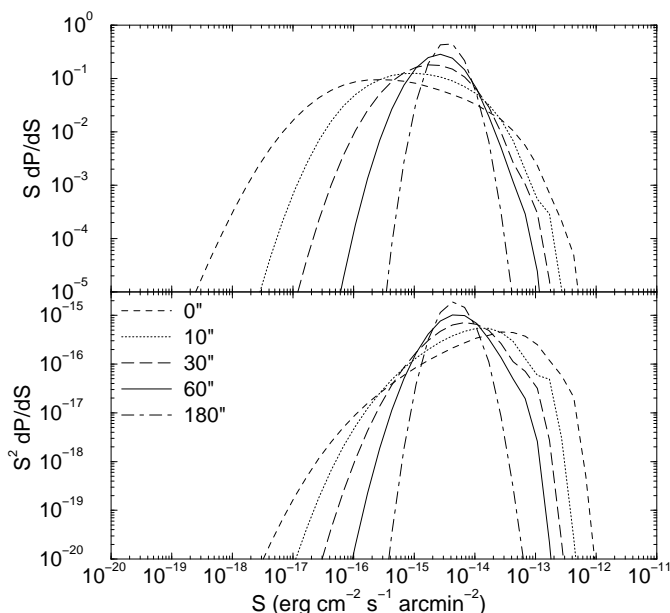


FIG. 6.— The distribution function for the L50+ simulation in the 0.5 to 2.0 keV band. In computing the distribution function, we have used a variety of Gaussian smoothing lengths, ranging from no additional smoothing up to 3 arcminutes.

We note that a single smoothing length is probably not the most efficient use of the data. A reasonable way to ensure constant signal-to-noise for all measured surface-brightness values would be to introduce an adaptive smoothing algorithm. This would preserve the high end of the distribution where the smoothing length would remain small, while introducing the minimum amount of smoothing in the low end.

3.3. Cooling and non-gravitational heating

There are two physical processes which we have so far neglected in these simulations. One of these is radiative cooling, which will have two contradictory effects. The first will be to increase the density of some of the X-ray emitting gas, since gas which cools will tend to be compressed. This will enhance the emissivity and hence the diffuse background. On the other hand, if the gas cools sufficiently rapidly that it never gets heated to X-ray emitting temperatures (or only briefly to such temperatures), then the energy will be emitted at other wavelengths, leading to a decrease in the diffuse X-ray background. To follow this process numerically is a computationally demanding task, since the simulation must resolve scales from below a kpc to 50 Mpc, accompanied with high mass resolution. Due to this difficulty, we are unable to investigate this process numerically. We simply note that it remains a viable mechanism for decreasing the X-ray background level to match observations (e.g. Bryan 2000; Croft et al. 2000).

The other physical process is feedback from the stellar systems within galaxies, primarily supernovae. Although we cannot follow the formation of galaxies and stars in detail for the same reasons described above, we can investigate simple energetic prescriptions which mimic the more complicated physics. Perhaps the most simplified way to account for the effect of feedback is to imagine it occurring at a single epoch with uniform efficiency in terms of energy per baryon. Exactly this prescription (or slight modifications thereof) has been modeled in a number of recent papers and seems to well account for the observed slope of the luminosity-temperature relation of groups and clusters of galaxies (Cavaliere, Menci & Tozzi 1997; Wu, Fabian & Nulsen 2000a; Valageas & Silk 1999; Loewenstein 2000). Although there is some disagreement on exactly how much heating is required, typical values are around 1 keV per baryon. We repeat two simulations but add 1.5 keV per particle (suddenly) at $z=3$. We will loosely refer to these as “feedback” simulations, and designate them as L50f+ and L50f-.

Heating results in a substantial decrease in the predicted mean diffuse X-ray background (see Table 1). The effect on the distribution function is extremely strong, as shown in Figure 7 for the 0.5 to 2.0 keV band. Due to the increase in temperature of the low density material in filaments, there is enhanced emissivity (within the band) in these regions and hence fewer low surface brightness pixels. The input of energy in dense regions results in a decrease in the density in those regions (groups become “puffier”). This decreases the number of high-brightness pixels. Together these changes result in a much more peaked distribution, so that most pixels have a surface brightness around 10^{-16} erg cm $^{-2}$ s $^{-1}$ arcmin $^{-2}$. On the other hand, the distribution is nearly flat in $S^2 dP/dS$ so that a wide range contributes to the mean value of the diffuse background, \bar{S} .

In this figure, we also plot the results for two “feedback” simulations with different resolutions. Clearly, the same numerical effects are operating as before. This is reflected in the systematic increase in the predicted mean flux with resolution seen in Table 1.

The effect of feedback is also very striking in the other band. Again, the distribution is strongly peaked, and the mean background decreases substantially. Also as before, the effect of resolution is such that we can only predict a minimum mean surface brightness from diffuse gas. However, as we will see in section 3.5, even this lower limit is quite restrictive.

The feedback prescription adopted here is quite simple — 1.5 keV of extra energy per baryon everywhere at $z = 3$. If the energy input in the real universe is concentrated around galaxies, then it may be biased towards generally high density regions. This should not change the behaviour on the high S end of the distribution (or on the mean flux), but may reduce the size of the effect at the low surface-brightness end, blunting the highly peaked structure seen in the upper panel of Figure 7.

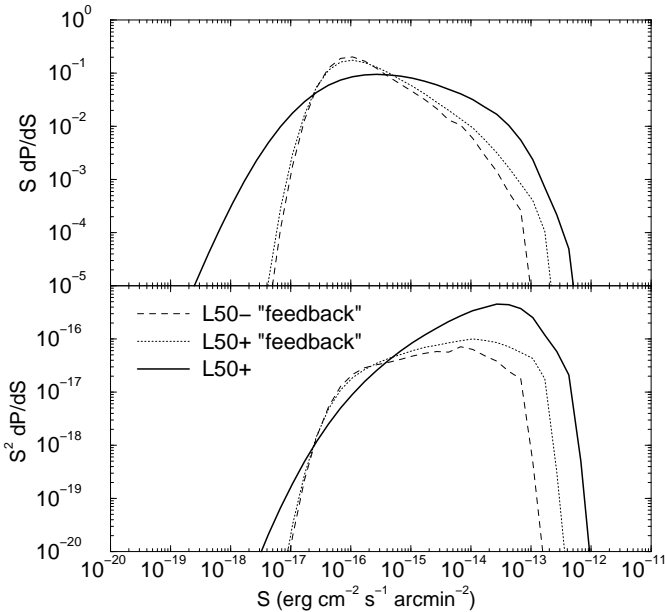


FIG. 7.— The 0.5-2.0 keV surface brightness distribution function for the L50+ and L50- simulations (differing in resolution) with and without the addition of 1.5 keV per baryon at $z=3$. The top and bottom panels have the same meaning as in Figure 2.

3.4. Where is the gas that emits the diffuse X-ray background?

Figure 1 shows the surface brightness map from one of the simulation volumes, and provides some hints as to where the emission come from. Clearly, the filaments which, at $z = 0.4$, have typical surface brightness values of around 10^{-16} - 10^{-18} $\text{erg cm}^{-2} \text{s}^{-1} \text{arcmin}^{-2}$ fall at the very low end of the expected distribution. As discussed in Voit, Evrard & Bryan (2000), this makes them very difficult to see due to confusion from other diffuse sources. This is in addition to the background from AGN and other point sources (see also Pierre, Bryan & Gastaud 2000). On the other hand, the centers of the clusters and groups provide the pixels with the highest surface-brightness.

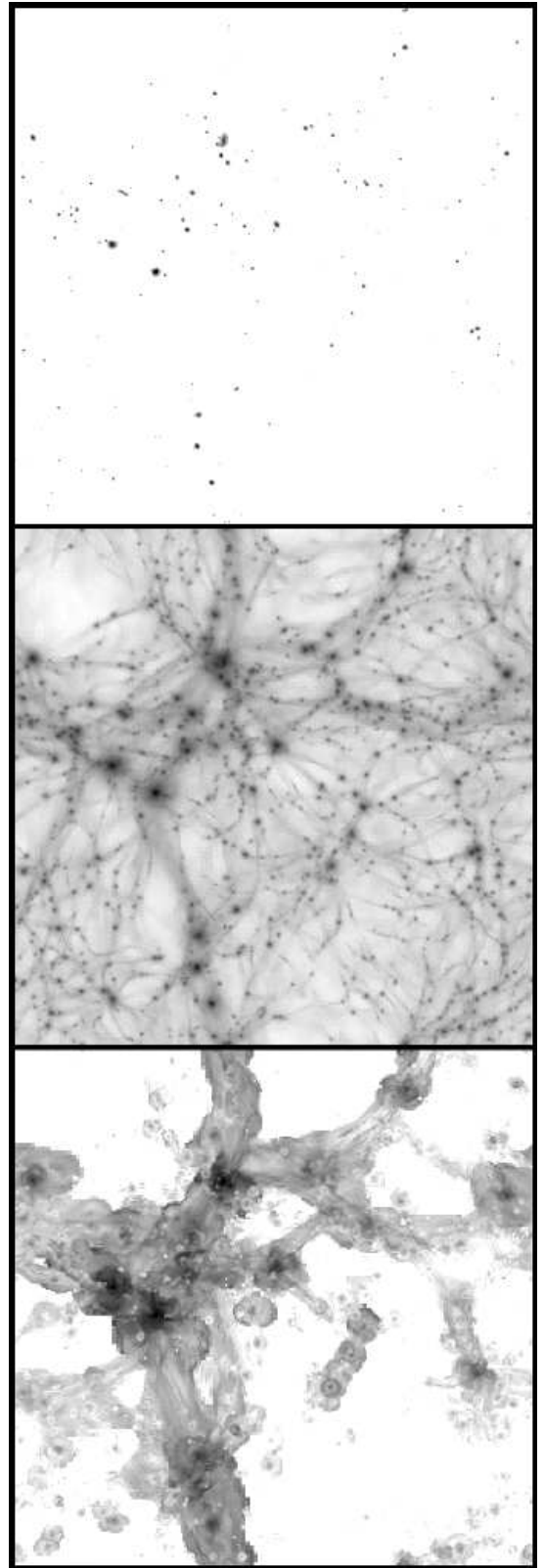


FIG. 8.— The top panel shows the 0.5-2.0 keV X-ray surface brightness map from a region $50 h^{-1}$ Mpc on a side at redshift $z = 0.4$ and line-of-sight distance $\Delta z = 0.02$. The greyscale is a stretch from 8.5×10^{-16} to 8.5×10^{-14} $\text{erg cm}^{-2} \text{s}^{-1} \text{arcmin}^{-2}$, a range which is responsible for 75% of the total flux. For a larger stretch of the same region, showing filaments, see Figure 1. The second frame shows a logarithmic greyscale map of the baryonic density and the bottom shows the (emission-weighted) temperature map, ranging from 10^6 to 5×10^7 K.

While this gives a qualitative answer, it would be useful to know if collapsed objects contribute the majority of the emission, and if so, what size group or cluster is primarily responsible. We answer these questions in two ways. The first is to pick out the surface brightness levels that are responsible for most of the flux. In Figure 8, we show the same simulated volume as in Figure 1, but now highlighting the regions for which the surface brightness lies between $S = 8.5 \times 10^{-16}$ and 8.5×10^{-14} $\text{erg cm}^{-2} \text{s}^{-1} \text{arcmin}^{-2}$. All together, these pixels account for 75% of the total flux emitted from the entire volume. Also shown is a map of the projected baryonic density and the (emission-weighted) temperature. Clearly, most of the flux comes from collapsed regions and not from filaments. This is despite the fact that a large majority of the gas is in filaments and diffuse structures. This implies that the gas distribution is iceberg-like: only a small fraction of it is easily visible.

Having determined that most of the emission comes from collapsed objects, it is of interest to determine what range of objects are primarily responsible for the emission. Although it is clear that larger objects tend to have a higher surface brightness, they are also rarer. In Figure 9, we show the relation between mean surface brightness and luminosity-weighted temperature (closely related to mass) for objects identified in the same simulation volume discussed above. The objects are identified in three-dimensions with the hop halo finder algorithm (Eisenstein & Hut 1999). The virial mass (M_{200}) is defined as all the mass within a sphere of radius r_{200} , within which the mean density is 200 times the critical density. The mean surface brightness S within the virial radius of the object (r_{200}) is given by $L/(4\pi^2 r_{200}^2 (1+z)^4)$ and L is the luminosity in the energy band of interest (defined in the observer's frame).

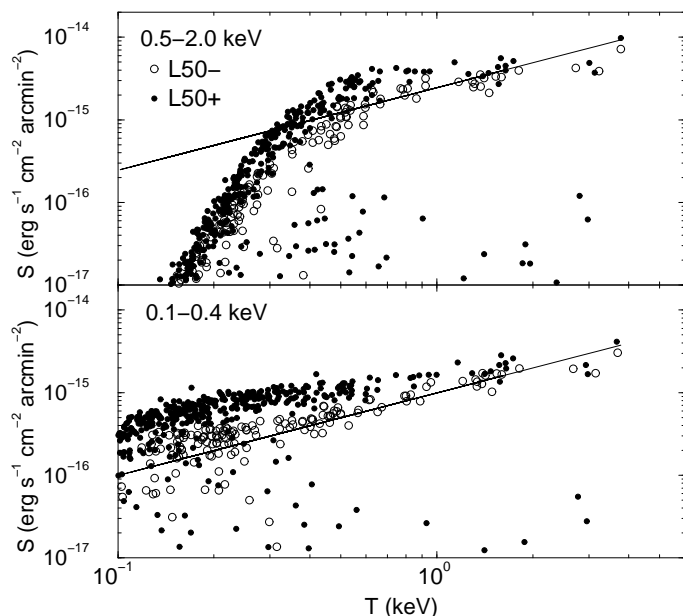


FIG. 9.— The mean surface brightness plotted against (luminosity-weighted) temperature for groups and clusters identified in the L50+ and L50- simulation at $z = 0.4$. The top panel shows the relation for the 0.5-2.0 keV band while the bottom shows the 0.1-0.4 keV band. Also plotted is the power-law relation based on scaling arguments and free-free emission (see text).

The figure shows more clearly the effect of resolution: while the largest clusters have the same predicted mean surface brightness in both simulations (which vary only in resolution), the smaller groups have systematically underpredicted emission. We can also check the surface-brightness-temperature ($S-T$) relation against simple analytic predictions. If we assume that all collapsed objects have the same profile when density is scaled by the critical density of the universe and radius is scaled by the virial radius, then the bolometric free-free luminosity should vary approximately as $L \sim T^2 H$ (see also Bryan & Norman 1998; Voit 2000). Combining this with $r_{200} \sim T^{1/2} H^{-1}$, we obtain:

$$S \sim TH^3(1+z)^{-4}. \quad (9)$$

Note the relatively slow evolution with redshift; for $\Omega = 1$, this becomes $S \sim T(1+z)^{1/2}$. This line is plotted in Figure 9. The well-resolved clusters climb above this line around 1 keV due to the increased importance of line-emission, which the simple analytic estimate does not include. Also, clusters with temperatures below about 0.2 keV produce very few photons in the 0.5-2.0 keV band. The points with low surface-brightness but high temperature represent relatively small halos which are in the processes of merging with larger systems.

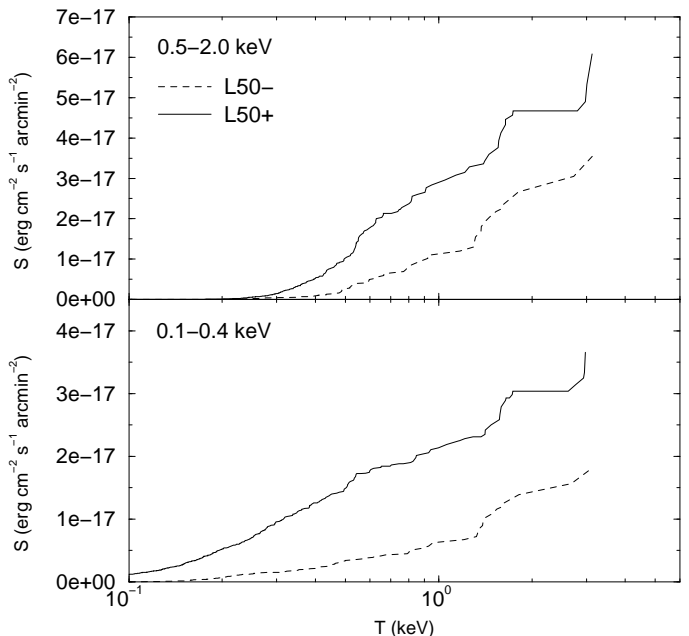


FIG. 10.— The cumulative contribution to the mean surface brightness from the clusters and groups identified in the same simulation volume discussed in the previous two figures. As usual, the top (bottom) panel shows the 0.5-2.0 (0.1-0.4) X-ray band. Within each figure, the solid and dashed lines show the effect of numerical resolution.

While useful, this figure still doesn't fully answer the question of what temperature range of halos is responsible for the X-ray background. This is addressed in Figure 10, which shows the cumulative contribution as a function of cluster or group temperature. Although a wide range of objects contribute, it is clear that the dominant contribution comes from halos with temperatures of order 1 keV ($\sim 10^{14} M_{\odot}$). For example, in the harder band, 50% of the flux is contributed by halos with temperatures greater

than 1.0 keV, while for the softer band, a similar fraction comes from groups with temperatures greater than 0.6 keV.

In each case, the total flux from identified halos is within a few percent of the flux as computed by summing all pixels of the surface-brightness map, indicating that filaments contribute a negligible fraction of the total flux. We should also point out that a substantial fraction of the background comes from relatively large, 2-4 keV objects, which are mostly missing in the smallest L20 simulations described in Table 1. This helps to explain why those simulations have a systematically different 0.5-2.0 keV surface brightness distribution function.

3.5. Comparison to observations

We can compare the predicted mean background fluxes from Equations 7 and 8 to those determined observationally. At 1 keV, the background has an intensity of about $I_X = 10 \text{ keV cm}^{-2} \text{ s}^{-1} \text{ sr}^{-1} \text{ keV}^{-1}$ with a spectral slope of $\alpha \approx 1.0$ (e.g. Wu et al. 1991; Gendreau et al. 1995; Barcons, Mateos & Ceballos 2000). At least 70% of this has been resolved into point sources (Hasinger et al. 1998; Giacomoni et al. 2000) and so does not originate in the diffuse gas of interest here. Therefore, we can convert this into an upper limit on the observed diffuse background; in the 0.5-2.0 keV band, this becomes:

$$S_{0.5-2.0}^{obs} < 5.0 \times 10^{-16} \text{ erg cm}^{-2} \text{ s}^{-1} \text{ arcmin}^{-2}. \quad (10)$$

From a review of shadowing experiments conducted by ROSAT, Warwick & Roberts (1998) found a mean background intensity in the 0.1-0.4 keV band (i.e. at 0.25 keV) of $20\text{-}35 \text{ keV cm}^{-2} \text{ s}^{-1} \text{ sr}^{-1} \text{ keV}^{-1}$, and that at least 80% of this was resolved into background sources. Assuming a spectral slope of $\alpha = 2$ (e.g. Gendreau et al. 1995; Barber, Roberts & Warwick 1996).

$$S_{0.1-0.4}^{obs} < 3.0 \times 10^{-16} \text{ erg cm}^{-2} \text{ s}^{-1} \text{ arcmin}^{-2}. \quad (11)$$

A reasonable extrapolation of AGN properties indicates that the likely upper limit to the diffuse background in this band is $4 \text{ keV cm}^{-2} \text{ s}^{-1} \text{ sr}^{-1} \text{ keV}^{-1}$ (Wu, Fabian & Nulsen 2000b), or $1.9 \times 10^{-16} \text{ erg cm}^{-2} \text{ s}^{-1} \text{ arcmin}^{-2}$.

Comparing these observations to the predicted values, it's clear that unless $\Omega_b h^2$ is far lower than the value we expect, the predicted background is larger than that observed. Even for the case with 1.5 keV of feedback, we would have to reduce the baryon fraction by 60%, to $\Omega_b h^2 = 0.011$, considerably below essentially all estimates (Burles et al. 1999). Reducing the assumed metallicity of the gas ($Z = 0.3$ of solar) would trim the predicted background somewhat, but since most of the flux comes from objects in the 1-3 keV range, where the metallicity is relatively well measured, there does not appear to be much room for maneuver.

In order to get an idea of how much feedback would be required to match observations, we performed two additional experiments. In one, we added the energy at $z = 1$ instead of $z = 3$ as would be required in order not to violate the IGM temperature constraints from Ly α clouds (e.g. McDonald et al. 2000; Schaye et al. 1999; Bryan & Machacek 2000). This actually resulted in an increased diffuse background, mostly because the effect is larger when

energy is added at lower densities, before the clusters and groups have fully formed. We speculate that adding energy earlier ($z > 3$) would be more efficient; however, it's not obvious what physical mechanism could provide so much energy so early.

We also examined the effect of increasing the feedback energy to 4.5 keV instead of 1.5 keV (at $z = 3$). For the low-resolution simulation (L50-), this resulted in a soft background of $1.9 \times 10^{-16} \text{ erg cm}^{-2} \text{ s}^{-1} \text{ arcmin}^{-2}$, somewhat below the most conservative observed limit quoted above. Since we expect about a factor of two increase in going to the L50+ resolution level (which would push the predicted background above even the conservative limit), it seems likely that a substantial amount of heating (at least 5 keV per particle) will be required. It should be stressed that this energy input occurs everywhere in our model, but it is certainly possible and even likely that energy would be more efficiently liberated (by star formation for example) in high-density regions than low-density regions. This would decrease the total energy budget required.

3.6. Comparison to previous work

The first paper to make specific predictions about the distribution of the soft X-ray background was an ambitious work by Scaramella, Cen & Ostriker (1993) who used numerical simulations to generate artificial maps of the X-ray background at 1 and 2 keV (as well as the Sunyaev-Zel'dovich y parameter). Because of numerical limitations, they were forced to use a more complicated chaining method of the boxes as well as being unable to check the convergence properties of the result. Their predicted mean background intensity was $I_X = 0.02 \text{ keV cm}^{-2} \text{ s}^{-1} \text{ sr}^{-1} \text{ keV}^{-1}$ at 1 keV, much lower than found here. Although it is possible that the different cosmological model (a closed $\Omega = 1$ CDM variant) played a role, there are two significant differences. One is that they removed the brightest pixels under the assumption that they would not be counted by observers; the second stems from the substantially lower resolution available at the time. Their spatial resolution was typically five times worse than used here and given the sensitivity on resolution we have highlighted earlier, this might explain the discrepancy. Still, they found a profile at the high end, $SdP/dS \sim S^{-1.8}$, which adequately matches the appropriate part of our distribution. The reason for this is given in Voit & Bryan (2001).

The mean background from diffuse gas (although not the distribution function itself) was calculated in an approximate fashion by Pen (1999). He used numerical simulations to determine the mean clumping factor of the IGM and then adopted a mean temperature from the cosmic virial theorem to generate an estimate of the mean background, assuming a mean metallicity of 0.25 solar. He found that numerical simulations gave only a lower limit to the mean clumping factor but that this lower limit was substantially larger than implied by the observed background. This is in agreement with the results found here, that the predicted background is approximately an order of magnitude larger than observed, indicating the need for some sort of additional physics. Pen also estimated that if feedback is responsible, the required energy budget would be around 2 keV, a value somewhat smaller than derived here.

Wu, Fabian & Nulsen (2000b) employed a semi-analytic technique to compute the predicted amplitude and spectrum of the diffuse X-ray emission. Although most of their models included cooling, a model without cooling or stellar feedback produced a mean background level which is substantially in agreement with that found here. They argued that while cooling would help somewhat, additional heating would be required and derived an excess specific energy of about 1 keV per particle. This is substantially lower than what we find in this paper; however, Wu, Fabian & Nulsen also included a treatment of cooling, making the comparison more difficult.

More recently, Davé et al. (2000) looked at the distribution of the warm-hot intergalactic medium (WHIM) and without performing a full calculation speculated that the WHIM gas would not overproduce the X-ray background. Here, we have shown that without additional heating or cooling this is not the case (although we should note that most of the simulations analyzed in that paper did model cooling and stellar feedback).

Finally, as this paper was in the late stages of preparation, two preprints appeared (Croft et al. 2000; Phillips, Ostriker & Cen 2000) using simulations to perform a full calculation of the X-ray background similar to that done here. The two papers use different simulation methods but similar physical models (radiative cooling and a simple feedback). They both concluded that the predicted background from diffuse gas is within the observed bounds, a result which at first appears to contradict this paper. There are several possible resolutions to this apparent conflict.

The first we examine is resolution and box size: in this paper we have carefully controlled for both of these effects, demonstrating that although a relatively modest simulation volume will produce a good estimate of the background (at least for the softer bands), numerical resolution is very important. Phillips, Ostriker & Cen (2000) have good mass resolution but relatively poor spatial resolution: they use a dark matter particle mass of $9 \times 10^9 M_\odot$, but a fixed cell size of only $195 h^{-1}$ kpc. A direct comparison is difficult since the algorithm differs from that used here; however, experience with such simulations (Bryan & Norman 1998) indicates that this cell size would lead to a significant underprediction of the luminosity for a simulation without cooling or radiative feedback. However, it is possible that this resolution is sufficient when these two processes are also included. Croft et al. (2000), using a smoothed-particle hydrodynamics technique, have both high spatial and mass resolution ($7 h^{-1}$ kpc minimum smoothing length and $7 \times 10^9 M_\odot$ dark matter particle mass). According to the results presented here, this should be sufficient resolution to obtain a reasonable estimate of the diffuse X-ray background. This, combined with the fact that the two groups produced similar results with different techniques, makes it unlikely that resolution and box size are playing a large role.

However, it is important to recognize that both Croft et al. and Phillips et al. included radiative cooling and feedback. Since the cosmological models were quite similar and previous comparisons between the different simulation techniques have produced similar results (Davé et al. 2000), the difference is probably due either to cooling or feedback. Although there are still many uncertainties, it

appears unlikely that feedback is the culprit since — as Croft et al. note — in SPH simulations the energy is liberated in dense regions and quickly radiated away. This would be consistent with the (unrealistically?) large levels of feedback required in this paper to bring the predicted background down to the level of the observation limits.

This leaves cooling. Because of numerical difficulties in treating the steep density profiles that radiative cooling generates, Croft et al. used a post-processing step to separate the cold phase from the hot phase, substantially decreasing the density of the hot phase. This diminished the emission by a factor of 15, so clearly the treatment of cooling is extremely important. A prominent role for cooling has also recently been proposed as an explanation for the scaling properties of clusters and groups (Bryan 2000). In that work, it was suggested that the varying efficiency of cooling in groups and clusters creates an effective entropy floor (as is also observed). Although we cannot directly test the cooling hypothesis in this work, we can examine the effect of adopting an entropy floor. To test this, we set the density of the gas in virialized regions (defined as those regions for which the density is at least 200 times that of the mean density), such that the “entropy” is increased by a value $kT/n_e^{2/3} = 100 \text{ keV cm}^2$, where n_e is the electron density and T the temperature. If this is done, then the resulting X-ray background prediction in the 0.5-2.0 keV band drops below observed limits, although the 0.1-0.4 keV band is still marginal (see Voit & Bryan 2000 for more details).

4. CONCLUSIONS

In this paper, we have used numerical simulations of a popular Λ -dominated cosmology to predict the contribution of the hot diffuse gas to the X-ray background. We assumed a constant metallicity of 0.3 solar and examined two bands: 0.1-0.4 keV and 0.5-2.0 keV, computing the mean background as well as the surface bright distribution function. The simulations included dark matter and baryons but did not self-consistently model either radiative cooling or star formation. We did however, examine the general effect of energy injection due to star formation via a simplified model of uniform heating. In order to focus on the diffuse gas, we ignored the contribution from compact sources. The conclusions are as follows:

- The predicted mean diffuse background depends on the mass resolution of the simulation, systematically increasing as the resolution improved. Although we feel we are nearing numerical convergence, this implies that our results are lower limits to the mean background.
- The surface brightness distribution (dP/dS) in the 0.5-2.0 keV band is only weakly dependent on resolution, and that at the very highest surface brightness end (unfortunately, it is also this end which makes the primary contribution to the mean background). The softer 0.1-0.4 keV band is less well resolved and the entire distribution shifts with resolution.
- Smoothing causes the distribution function to peak at moderate surface brightness values. While slight smoothing (of only a few arcsecs) has only a small

effect, even 10" or 30" smoothing significantly modifies the shape of the distribution function.

- Although a substantial fraction of the baryonic mass is in the form of filaments or other low-density structures, the diffuse background overwhelming originates in groups and clusters. The 0.1-0.4 keV band comes from groups with a virial temperature of order 0.6 keV, while the harder 0.5-2.0 keV band originates in larger, 1.0 keV systems. However, in both cases, a wide range of objects contribute.
- Feedback modifies the shape of the distribution function. This occurs in large part because the additional energy inflates the core of clusters and groups, decreasing the emission from the brightest central regions and thereby suppressing the high end of the distribution function.
- Since the measured X-ray background has now been largely resolved into point sources, presumably almost entirely due to compact sources, this provides an upper limit to any possible contribution from diffuse gas. Our upper limit to the predicted mean distribution substantially exceeds this bound. This confirms the initial suggestions (Pen 1999; Wu, Fabian & Nulsen 2000b) that the hot gas in clusters and groups — in the absence of non-gravitational heating or radiative cooling — would overproduce the X-ray background.
- Including a simple form of feedback (a uniform 1.5 keV per particle injected at $z = 3$) reduces but does not eliminate the discrepancy. It seems likely that either (a) much more energy is required (at least 5 keV per particle), (b) the energy is injected at substantially higher redshift than three, or (c) additional

physical processes are at play. This could be a more complicated form of feedback which operates in a substantially different fashion than simple energy injection, or it could be that a substantial fraction of the gas in groups cools, reducing the luminosity of such groups (Bryan 2000). If this latter suggestion is correct, it would be consistent with the differences between our results and another recent simulation (Croft et al. 2000) which included radiative cooling but did not exceed the observational limits.

While this work is a significant step forward in the study of the diffuse X-ray background, much more work remains to be done. This includes understanding the effect of realistic energy and metal injection on the IGM. It will be very important to understand the role of cooling on the state of the hot gas in groups and clusters.

The X-ray background contains a wealth of potential information relating to the diffuse, cosmologically distributed gas that hierarchical cosmological models predict. This information is difficult to interpret since it requires removing the contribution from point sources and accounting for the effect of the lower number of photons coming from areas of low intrinsic surface brightness. However, a careful measurement of the surface brightness distribution function would constrain the thermal history of the gas, helping us to understand the energy input from supernovae and AGN.

Support for GLB was provided by NASA through Hubble Fellowship grant HF-01104.01-98A from the Space Telescope Science Institute, which is operated by the Association of Universities for Research in Astronomy, Inc., under NASA contract NAS6-26555. Some simulations in this paper were performed at the National Center for Supercomputing Applications (NCSA).

REFERENCES

- Barber, C.R., Roberts, T.P., Warwick, R.S. 1996, MNRAS, 282, 157
 Barcons, X., Fabian, A.C., & Rees, M.J. 1991, Nature, 350, 685
 Barcons, X., Mateos, S. & Ceballos, M.T. 2000, MNRAS, 316, L13
 Boyle, B.J., Shanks, T., Georgantopoulos, L., Stewart, G.C., Griffiths, R.E. 1994, MNRAS, 271, 639
 Bryan, G.L., Norman, M.L., Stone, J.M., Cen, R., Ostriker, J.P. 1995, Comput. Phys. Comm., 89, 149
 Bryan, G. L. 1999, Computing in Science & Engineering, March - April 1999, 46
 Bryan, G.L. & Machacek, M. 2000, ApJ, 534, 57
 Bryan, G. L. & Norman, M. L. 1997a, in ASP Conf. Ser. 123, Computational Astrophysics, eds. D. A. Clarke & M. J. West, (San Francisco: ASP), 1998, p. 363
 Bryan, G. L. & Norman, M. L. 1998, ApJ, 495, 80
 Bryan, G.L. 2000, ApJ, in press
 Burles, S., Nollett, K.M., Truran, J., N. Turner, S.T., 1999 Phys. Rev. Lett., 82, 4176
 Cavaliere, A. Menci, N. & Tozzi, P. 1997, ApJ, 484, L21
 Colella P., Woodward P.R., 1984, J. Comp. Phys. 54, 174
 Croft, R.A.C., Di Matteo, T., Davé, R., Hernquist, L., Katz, N., Fardal, M.A. & Weinberg, D.H. 2000, preprint, astro-ph/0010345
 Davé, R., Cen, R., Ostriker, J.P., Bryan, G.L., Hernquist, L., Weinberg, D., Norman, M.L., O'Shea, B. 2000, ApJ, in press
 Eisenstein, D. J. & Hu, W. 1998, ApJ, 496, 605
 Eisenstein, D. J. & Hut, P. 1998, ApJ, 498, 137
 Gendreau, K.C., Mushotzky, R., Fabina, A.C., Holt, S.S., Kii, T., Serlemitsos, P.J., Ogasaka, Y., Tanaka, Y., Bautz, M.W., Fukazawa, Y., Ishisaki, Y., Kohmura, Y., Makishima, K., Tashiro, M., Tsusaka, Y., Kunieda, H., Ricker, G.R., Vanderspeck, R.K. 1996, PASJ, 47, L5
 Giacconi, R., Rosati, P., Tozzi, P., Nonino, M., Gasinger, G., Norman, C., Bergeron, J., Borgani, S., Gilmozzi, R. & Zheng, W. 2000, preprint, astro-ph/0007240
 Hasinger, G., Burg, R., Giaconi, R., Hartner, G., Schmidt, M., Trümper, J. & Zamorani, G. 1993, A&A, 275, 1
 Hasinger, G., Burg, R., Giacconi, R., Schmidt, M., Trümper, J. & Zamorani, G. 1998, A&A, 329, 482
 Loewenstein, M. 2000, ApJ, 532, 17
 McDonald, P., Miralda-Escudé, J., Rauch, M., Sargent, W.L.W., Barlow, T.A., Cen, R. 2000, preprint (astro-ph/0005553)
 Mushotzky, R.F., Cowie, L.L., Barger, A.J. & Arnaud, K.A. 2000, Nature, 404, 459
 Peebles, P.J.E. 1993, Principles of Physical Cosmology (Princeton: Princeton University Press), p. 312
 Pen, U.L. 1999, ApJ510, L1
 Phillips, L.A., Ostriker, J.P., Cen, R. 2000, ApJ, submitted, astro-ph/0011348
 Pierre, M. Bryan, G., & Gastaud, R. 2000, A&A, 356, 403
 Raymond, J.C. & Smith, B.W. 1977, ApJS, 35, 419
 Scaramella, R., Cen, R., & Ostriker, J.P. 1993, ApJ, 416, 399
 Schaye, J., Theuns, T., Leonard, A., Efstathiou, G., 1999, MNRAS, 310, 57
 Soltan, A. M., Freyberg, M., Hasinger, G., Miyaji, T., Treyer, M., Trümper, J. 1999, A&A, 349, 354
 Valageas, P. & Silk, J. 1999, A&A, 350, 725
 Voit, G.M. 2000, ApJ, in press
 Voit, G.M., Evrard, A., Bryan, G.L., ApJL, submitted
 Voit, G.M., Bryan, G.L., ApJL, submitted
 Warwick, R.S. & Roberts, T.P. 1998, Astronomische Nachrichten, 319, 59
 Wu, K.K.S., Fabian, A.C. & Nulsen, P.E.J. 2000a, MNRAS, 318, 889
 Wu, K.K.S., Fabian, A.C. & Nulsen, P.E.J. 2000b, preprint, astro-ph/9910122
 Wu, X., Hamilton, T., Helfand, D.J. & Wang, Q. 1991, ApJ, 379, 564